



Influence of Particle Velocities on Adhesion Strength of Cold Spray Inner Diameter Coatings

Joachim Meeß¹ · Manuel Anasenzl¹ · Ralf Ossenbrink² · Vesselin Michailov²

Submitted: 22 April 2022 / in revised form: 20 June 2022 / Accepted: 25 June 2022 / Published online: 7 July 2022
© The Author(s) 2022

Abstract Due to the recent developments of hardware components and the hereby resulting ability to increase process parameters, the application area of the cold gas spray technology is expanding quickly. The present research focuses on the influence of working gas pressure and working gas temperature on the adhesive strength of inner diameter coatings, which were produced with two different alloy steel powder variants. Gas pressure and gas temperature were varied in four different parameter sets. At first, the powder variants were examined for morphology and particle size distribution. Secondly, the influence of four different process parameters on the achievable particle velocity was measured. In addition, the arithmetical mean height (S_a) of the coating was measured in order to determine the effect of the four parameter sets on the achievable surface roughness. Furthermore, the impact of the process parameters on the steel particles' penetration depth into the aluminum substrate was examined. Finally, adhesion strength measurements of the inner diameter coatings were carried out. The results reveal that with rising process parameters, the particle velocity increases,

and the achievable surface roughness is lowered. It was also shown that the penetration depth of the particles into the substrate increases with increasing particle velocity. In addition, this study demonstrated a dependence of the process parameters on the adhesion strength for inner diameter coatings.

Keywords adhesion strength · cold gas spraying (cgs) · cylinder block application · inner diameter coating · particle velocity

Introduction

Cold gas spraying (CGS) is a coating technology which was developed in the mid-1980s at the Institute of Theoretical and Applied Mechanics of the Russian Academy of Science in Novosibirsk (Ref 1). In the CGS process, powder particles with a particle diameter (usually 5–50 μm) are accelerated to high particle velocities (300–1200 m/s) using a de Laval nozzle (Ref 2). The particles are deposited by plastic deformation on impact with the substrate or coating. CGS is a solid-state process in which the particle temperature is always well below the melting point of the feedstock powder (Ref 3, 4). Due to very high particle velocities, the substrates do not have to be specially roughened before starting the coating process, whereas in other thermal coating technologies samples must be prior activated to ensure a solid adhesion between the coating and substrate (Ref 2). Gas pressure and gas temperature are the main parameters affecting the particle velocities and thus also the achievable adhesion strengths. In general, the higher the applied process parameters (gas pressure and gas temperature) in the fabrication step of the coating, the higher the particle velocities at the nozzle

✉ Joachim Meeß
joachim.meess@bmw.de

Manuel Anasenzl
manuel.j.anasenzl@bmw.de

Ralf Ossenbrink
ralf.ossenbrink@b-tu.de

Vesselin Michailov
fg-fuegetechnik@b-tu.de

¹ BMW AG, Ohmstr. 2, 84030 Landshut, Germany

² Department Joining and Welding Technology, BTU Cottbus–Senftenberg, Konrad-Wachsmann-Allee 17, 03046 Cottbus, Germany

outlet. In addition to gas pressure and gas temperature, the position of the particles in the gas stream and the particle size and particle morphology of the feedstock powder can also influence the particle velocity (Ref 5-7). Previous studies have shown that increasing particle velocities ensure that the adhesion strength of the coating on the substrate continues to increase. In general, the higher the particle velocity, the higher the deformation of the deposited particles and the higher the adhesion strength (Ref 5, 8, 9). For instance, an adhesion strength of more than 60 MPa can be achieved with powder 316L on an aluminum substrate (Ref 9-11).

According to the current state of the art, gas temperatures of up to 1000 °C can be achieved in combination with 60 bar gas pressure (Ref 12). Previous research has shown that CGS technology can be used for inner diameter coatings, particularly for the surface coating of cylinder bores in the automotive industry. In these investigations, substrates were not specially roughened, while adhesion strengths of the fabricated coatings were still sufficient (Ref 12, 13). Furthermore, it is known that only particles with a velocity above the critical velocity can be deposited. Therefore, no deposition of particles occurs below the critical velocity (Ref 14-17). Experimental and theoretical studies have shown that the critical velocity depends on the properties of the powder and the substrate, e.g., particle size and morphology, particle temperature, particle oxygen content and substrate preparation (Ref 18-23). Although the mechanisms of particle adhesion are not yet fully understood, it can be assumed that the adhesion process is strongly dependent on the impact velocity of the particles, which results from spraying conditions (Ref 24, 25). High gas and particle temperatures and high particle velocities improve adhesion (Ref 26). In addition, former experiments revealed that the substrate surface roughness had an influence on the adhesion strength of the CGS coating. The rougher the surface, the higher the deformation of the particles on impact and thus the adhesion strength of the coating to the substrate (Ref 27).

The aim of this study is to determine the influence of different process parameters (working gas pressure and working gas temperature) on the particle velocity and the resulting adhesion strength of two different alloy steel powders with different chemical compositions, particle sizes and morphologies using a CGS system for inner diameter coatings. Initially, different powder variants were examined for particle size and particle morphology. Afterward, the impact of various process parameters on particle velocities and the achievable surface roughness of the coating was investigated. Furthermore, the penetration depth of the steel particles into the substrate was evaluated. Finally, the adhesion strength of the inner diameter CGS

coating on the substrate and its influencing variables were analyzed.

Experimental Procedure

Cold Spray Experimental Setup

In this study, a standard 6/11 EvoCSII cold spray system and an angled head developed by Impact Innovations GmbH (Rattenkirchen, Germany) for components with an inner diameter > 70 mm were used to prepare the inner diameter coatings for adhesion strength measurements (Fig. 1). The gun rotates 360° and moves up and down. The spraying path (spiral) results from the travel speed and the rotating speed of the spray gun. The powder was fed into the process simultaneously using two powder feeders, which blasted the feedstock powder into just a single injection line. Utilizing this, the powder was immediately injected before the nozzle. An adapted convergent-divergent (De-Laval) nozzle with a length of 55 mm and an expansion ratio of 12.438 was installed into the angled head. The distance of 12 mm between the nozzle outlet and the substrate resulted in a spray spot diameter of 8 mm. Using this method, the nozzle is cooled with water to prevent clogging. Different parameter sets and feedstock

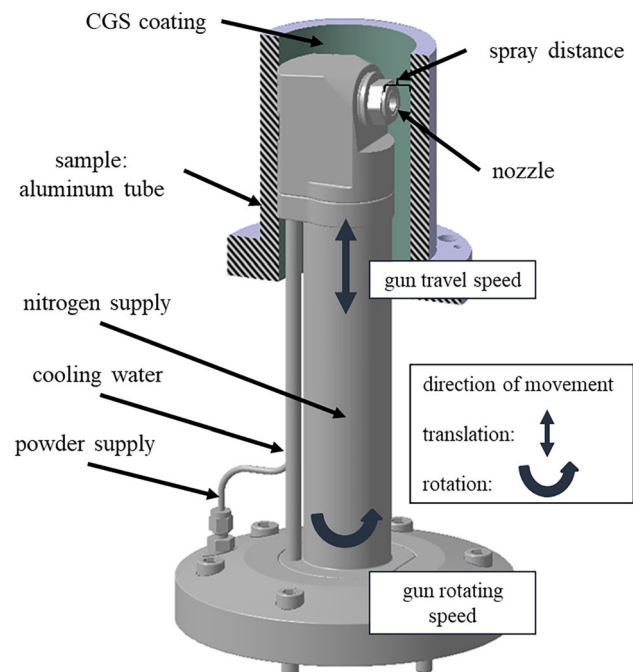


Fig. 1 Schematic display of the experimental setup for inner diameter coated cold gas spray coatings (based on (Ref 12)). Reprinted by permission from Springer Nature Customer Service Centre GmbH: Springer Nature, *Journal of Thermal Spray Technology*, Cold Gas Spray Inner Diameter Coatings and Their Properties, Joachim Meeß et al., Copyright 2022 (Ref 12)

powders led to different deposition efficiencies. Two iron-based powder types (316L and M3/2) with different morphologies, in terms of particle size distribution and chemical composition, were investigated as feedstock powders for CGS coatings. Powder 316L is a commercially available stainless steel powder from Sandvik Osprey, Ltd. (Neath, Great Britain), which is atomized using nitrogen gas. Powder M3/2 is a water-atomized tool steel powder with some carbides (MC & M6C) from Höganäs AB (Höganäs, Sweden). Table 1 shows the chemical compositions of the two alloy steel powder variants 316L and M3/2.

An aluminum liner (AlSi7MgCu0.5) with an inner diameter of 82.38 mm, a height of 146 mm and a wall thickness of 11 mm was used as a substrate. In order to achieve an approximately constant coating thickness of 350 μm, the powder feed rate or the gun travel speed has to be adjusted, since the deposition efficiency varies with different process parameters (gas pressure and gas temperature) and different powder variants (316L and M3/2). In these studies, the gun travel speed was adjusted, and the powder feed rate was maximized in all measurements to produce the fastest possible coating process and thus minimize the temperature effect of the process on the substrate. The gun travel speed in these investigation was 4 mm/s for powder M3/2 and 8 mm/s for powder 316L. Table 2 shows the detailed spraying conditions. In this research, the following different parameter sets were utilized (see Table 3).

Sample Characterization

Scanning electron micrographs (SEM) images were taken with a Zeiss EVO 60 XVP in order to evaluate the morphology of the powder particles. In addition, the two alloy

steel powders were characterized by dynamic image analysis using a CAMSIZER® X2 from Microtrac Retsch GmbH (Haan, Germany). In particular, a volume-based dry measurement approach for the particle size distribution was applied with the aim to quantify the nominal particle diameter (x_{area}) and circularity (C) of the particles.

Particle diameter x_{area} displays the equivalent particle diameter, which corresponds to the diameter of an equal-area circle. This parameter is suitable for comparing the CAMSIZER® X2 results with a laser scattered light analysis. Circularity C indicates the roundness C , which is obtained from the particle circumference U and the particle area A . In this regard, perfect circles or spheres have a roundness of 1. For all other shapes, the roundness is < 1 .

$$C = \sqrt{\frac{4\pi A}{U^2}} \tag{Eq 1}$$

The influence of different parameter sets on the particle velocities was measured with a cold spray meter from Tecnar Automation Ltée (Saint-Bruno-de-Montarville, Canada). The distance of the measuring point to the nozzle outlet was 12 mm.

The surface roughness of the inner diameter coating was measured with a MarSurf CP Select from Mahr GmbH (Göttingen, Germany) at 3 different locations (top, center, bottom) on the liner. In order to assess the influence of various process parameters on the surface roughness, the arithmetic mean height (Sa) was measured according to DIN EN ISO 25178. The parameter A represents the considered area of the coating, whereas $z(x, y)$ illustrates the profile height. In this study, the measuring area covered an area of 3 mm x 3 mm.

$$Sa = \frac{1}{A} \iint_A |z(x, y)| dx dy \tag{Eq 2}$$

Cross sections of the cylinders were made after the coating processes with which the steel particles' penetration depths were measured. The micrographs were taken in the midsection of the liner at 0°, 90°, 180° and 270°. For this purpose, the cylinder liners were cut into small slices using a diamond blade. The samples were cold embedded

Table 1 Chemical compositions of powder 316L and M3/2

Element	Chemical composition (%)	
	316L	M3/2
Iron (Fe)	61.0	72.1
Chromium (Cr)	18.7	4.0
Nickel (Ni)	12.7	...
Tungsten (W)	...	6.0
Vanadium (V)	...	5.6
Molybdenum (Mo)	2.9	6.6
Carbon (C)	2.5	4.8
Manganese (Mn)	1.4	0.3
Oxygen (O)	0.4	0.6
Silicon (Si)	0.4	...

Table 2 CGS spraying conditions

Gas type	N ₂
Working gas temperature (°C)	900 & 1000
Working gas pressure (bar)	50 & 57
Spray distance (mm)	12
Gun travel speed (mm/s)	4-8
Gun rotating speed (rpm)	120
Powder feed rate (cm ³ /min)	50.49

and successively grounded with silicon carbide abrasive paper. Subsequently, the cross sections were treated with polishing pastes to achieve a surface quality of up to $1\ \mu\text{m}$. Then, micrographs were taken using the Zeiss Axio Imager M2m from Carl Zeiss Microscopy Deutschland GmbH (Oberkochen, Germany). The porosity of the coating was determined by gray contrasts using Imagic IMS Image Processing V18Q4 software. The test area was $1\ \text{mm}^2$, and the thresholds were adapted to the coating: coating 316L between 0 and 140 and coating M3/2 between 0 and 60.

The adhesion strength measurements of various coatings were carried out using a PosiTest AT-A from DeFelsko Corporation (Ogdensburg, New York, USA). Figure 2(a) shows the coated cylinder surface with bonded dome-shaped stamps (dome radius of 41 mm), which were prepared for adhesion strength measurements. Figure 2(b) shows a cross section of the adhesive bond between the dome-shaped stamp and the CGS coating. The stamps were glued to the coated cylinder liner surface with an FM® 1000 epoxy resin adhesive film, which obtains a maximum strength of 70 MPa and was provided by HTK Hamburg GmbH (Hamburg, Germany). Removal measurements were carried out after a curing time of 1 h at $175\ ^\circ\text{C}$ in the oven. In these experiments, a glue thickness between $60\ \mu\text{m}$ and $90\ \mu\text{m}$ was required. With an electronically controlled hydraulic pump, which distributed an

even and continuous pull-off speed of $1.5\ \text{MPa/s}$, the stamps were then removed. Although this setup is not a standard test, it allows the measurement of the adhesion strengths directly on the cylindrical surface coating of the specimens. In contrast, the standard adhesion test (ASTM C633) for thermally sprayed coatings can only be used for specimen with a straight test surface and therefore is not suitable for measurements on internal coatings.

Results and Discussion

Powder Characterization

Figure 3 shows SEM images of the two powder variants. The particles of powder 316L are almost spherical with some satellites surrounding the powder particles. In contrast, powder M3/2 is irregular and elongated. These morphology types are a result of various powder manufacturing processes. In general, gas-atomized powder (316L) tends to be spherical and regular in shape, while water atomized powder (M3/2) has irregular powder particles (Ref 28).

The volume-related particle size distribution of the particles' diameter x_{area} of powder 316L and powder M3/2 is shown in Fig. 4 and 5. The particle size

Table 3 Four different parameter sets

Parameter set	Gas working pressure (bar)	Gas working temperature ($^\circ\text{C}$)
1	50	900
2	57	900
3	50	1000
4	57	1000

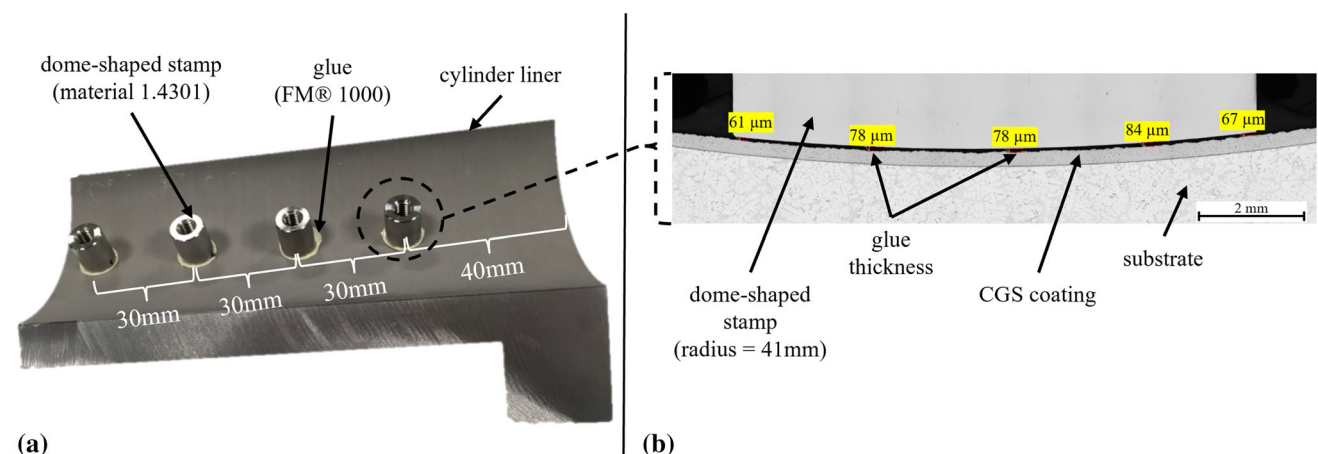


Fig. 2 (a) Coated cylinder surface with bonded dome-shaped stamp prepared for adhesion testing; (b) Cross section of the adhesive bond between the dome-shaped stamp and the CGS coating

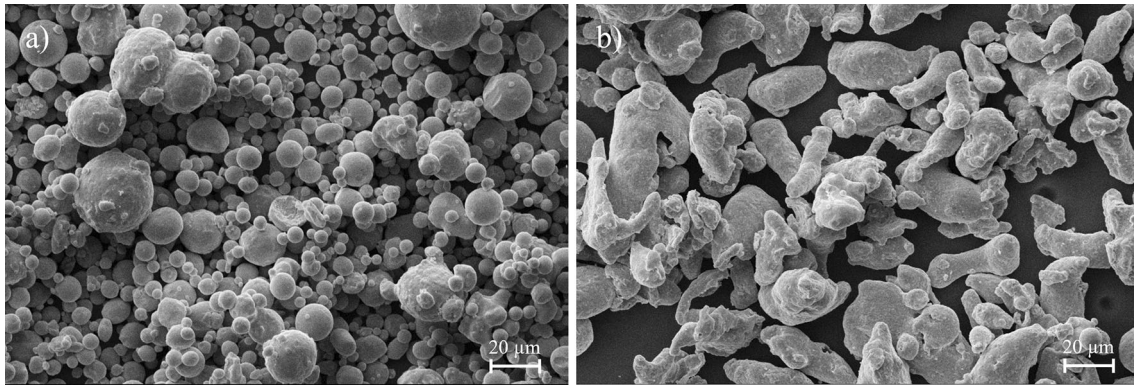


Fig. 3 SEM images of the powder used in the experiments: (a) 316L and (b) M3/2

Fig. 4 Particle size distribution of powder 316L

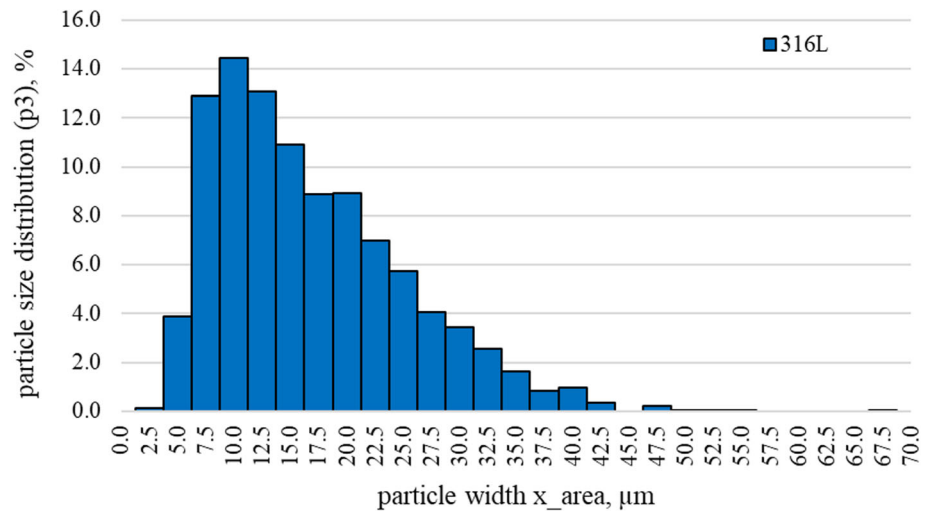
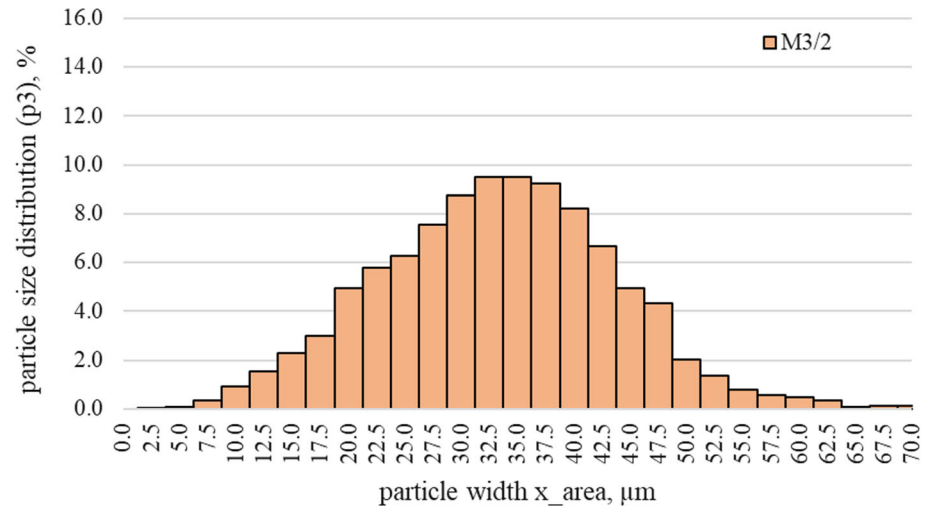


Fig. 5 Particle size distribution of powder M3/2



distribution of powder M3/2 ranges from 7.5 to 70.0 μm and is symmetrically distributed (gaussian distribution). Powder 316L has a non-symmetric distribution with a particle size distribution from 5 to 47.5 μm, whereas most particles show a size < 20 μm.

A summary of Fig. 3 and the roundness of the particles is displayed in Table 4 with the values d_{10} , d_{50} , d_{90} , C and apparent density. The different particle size distribution of the two powders is especially reflected in the value of $x_{area} d_{90}$. The $x_{area} d_{90}$ value of powder M3/2 is 37%

Table 4 Particle size d_{10} , d_{50} , d_{90} , circularity C and apparent density

Particle property	316L	M3/2
$x_{c \text{ min}} (d_{10})$ in μm	8.76	21.02
$x_{c \text{ min}} (d_{50})$ in μm	16.19	34.72
$x_{c \text{ min}} (d_{90})$ in μm	30.02	47.67
C	0.9387	0.8534
Apparent density in g/cm^3	3.1	2.6

higher than $x_{\text{area } d90}$ value of powder 316L. Furthermore, Table 3 shows the circularity C of the two powders and illustrates the difference between spherical and irregular particle shapes. The measured value C confirms the SEM images from Fig. 1 ($C_{316L} > C_{M3/2}$). Sphericity plays an important role in relation to particle velocity. A reduction in the sphericity ($C \downarrow$) of the powder particles leads to a significant increase in particle velocity (Ref 29). Due to a larger d_{90} value and a lower C value, the drag coefficient of powder M3/2 is higher than the one of powder 316L and, therefore, higher particle velocities should be expected (Ref 12, 30, 32). In addition, previous studies have shown that particle size and particle density have another important influence on particle velocity. The larger and heavier the particles, the lower the particle acceleration (Ref 33). The higher apparent density of 3,1 g/cm^3 for powder 316L has a negative effect on particle velocity compared to the apparent density of 2,6 g/cm^3 for powder M3/2.

A higher particle velocity leads to a higher particle deformation in the impact and thus reduces the surface roughness (Ref 8, 34). In addition, the stepover distance of the individual spray paths can have an influence on the surface roughness during coating. The swirling pitch is twice as large for powder 316L as for powder M3/2, which is due to the different gun travel speed (swirling pitch 4 mm per revolution for powder 316L and 2 mm per revolution for powder M3/2). The gun travel speed was adjusted that the same coating thickness was achieved with the same powder feed rate.

Previous research demonstrated the correlation between coating roughness and particle size: smaller particle diameters lead to lower CGS surface roughnesses (Ref 34). Furthermore, the mean roughness depth (R_z) of CGS inner diameter coatings after mechanical processing depends on the grain size of the feedstock powder (Ref 12). Thus, it can be said that the used particle size affects the surface roughness of the CGS coating. In these experiments, it is expected that the coatings of powder 316L have lower arithmetical mean heights (S_a) of the manufactured coating surfaces than the coatings of powder M3/2, since

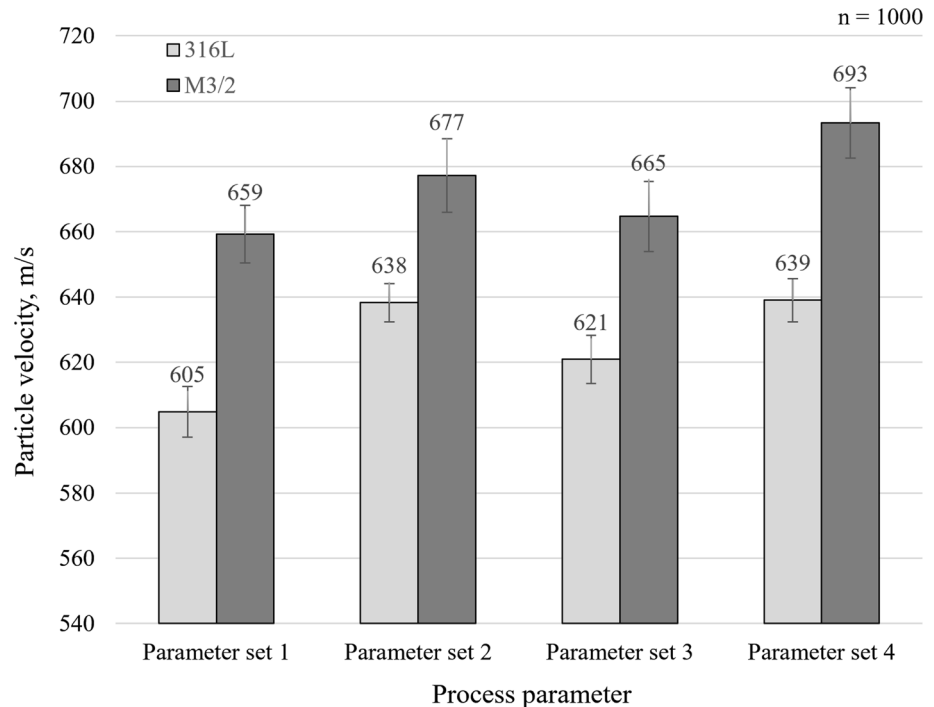
$x_{\text{area } d90}$ of powder M3/2 is 37% higher than $x_{\text{area } d90}$ of powder 316L.

Particle Velocity

Particle velocity measurements were carried out in order to investigate the influence of the four parameter sets (see Table 3) on the velocity of the two powder variants. Figure 6 shows that the average particle velocity of the two powder variants was lowest for the first parameter set and highest for the fourth parameter set. This result confirms previous studies which have shown that the particle velocity increases with rising working gas pressure and working gas temperature (Ref 12, 13, 35, 36). For all four parameter sets, the particle velocity of powder M3/2 was higher than the one of powder 316L. Moreover, the difference in particle velocities between the powder variants ranged from 6.1% in parameter set two (638 to 677 m/s) to 8.9% in parameter set one (605 to 659 m/s). Powder M3/2 has a slightly lower density (16% lower than 316L) and a larger $x_{\text{area } d90_{M3/2}}$ value ($d_{90_{M3/2}}$ 63% larger than $d_{90_{316L}}$). However, the heavier M3/2 powder particles compared to 316L are accelerated faster. This observation is partly due to the fact that the drag coefficient of the irregular particle shapes of powder M3/2 is higher than the one of the round particle shapes of powder 316L. As a result, the increased drag coefficient allows the particles to accelerate faster in the applied gas stream (Ref 12, 30, 32).

In the investigated parameter range of this study, it was shown that an increased gas pressure of 14% (7 bar difference between parameter set one and parameter set two) had a significant greater influence on the particle velocities than a 11% higher gas temperature (100 °C difference between parameter set one and parameter set three) for both powders. In addition, the percentage increase in velocity at a pressure increase of 7 bar was 2.7% for powder M3/2 and 5.5% for powder 316L. In contrast, the particle velocities increased by only 0.9% for powder M3/2 and 2.6% for powder 316L at a 100 °C difference of gas temperature. This is conclusive with previous studies, which have shown that working gas pressure has a greater effect on particle velocities than working gas temperature (Ref 13). The significant higher particle velocities of powder M3/2 ought to result in more substrate's deformation on impact than the slower accelerated particles of powder 316L (Ref 5). In addition to the particle size, the surface roughness of the CGS coating is also influenced by the particle velocity and the deformation of the particles upon impact. A lower particle velocity leads to a higher roughness of the coating (Ref 34). For this reason, an inner diameter coating with process parameter 4 (higher particle velocity) should have a lower arithmetical mean height (S_a) and a higher particle penetration depth into the

Fig. 6 Particle velocity at different gas temperatures and gas pressures. Powder variants used: 316L and M3/2. Number of measurements = n . Error bars represent the standard deviation (1 sigma)



substrate than an inner diameter coating with process parameter 1 (lower particle velocity).

In addition, for coatings with small standoff distance, it should be noted that a bow shock effect occurs between the nozzle exit and the substrate. It is known that the bow shock effect has a negative effect on particle velocity and slows down if the standoff distance is too small. This effect can already occur at a standoff distance of 60 mm and reduce the deposition efficiency by 40%. The influence of the bow shock effect is greater for non-spherical particles than for spherical particles due to the higher drag coefficient (Ref 37). For this reason, it is assumed that the bow shock effect also influenced the results in the present investigations. The bow shock effect could be one explanation for the fact that for powder M3/2 the gun travel speed has to be halved to achieved the same layer thickness as for powder 316L, although the measured particle velocity (without bow shock effect) was higher for powder M3/2 than for powder 316L.

Surface Roughness

Figure 7 shows the measured values of the arithmetical mean height (Sa) of the CGS coatings with powder 316L and powder M3/2 for all four parameter sets. In this matter, coatings with powder M3/2 had a significantly rougher surface than coatings with powder 316L. The arithmetical mean height (Sa) of the coating with powder M3/2 was between 68% (for parameter set four) and 90% (for parameter set one) above the arithmetical mean height (Sa)

of the coating with powder 316L. This is due to the larger and more irregular particle shapes of the feedstock powder M3/2, when compared to the feedstock powder 316L ($x_{\text{area } d90}$ M3/2 is 37% higher than $x_{\text{area } d90}$ 316L). The differences in surface roughnesses are illustrated by the 3D view of various fabricated surfaces in Fig. 8 and 9. In this study, the influence of the swirling pitch on the surface roughness was not investigated. Therefore, only the surface roughness values can be compared within one powder variant, since the pitch was the same. Although there is a clear difference in the surface roughness between the individual powder variants, which in this study is largely due to the particle size, the influence of swirling path must be investigated in further steps.

The results of this study confirm the observations from previous studies that the surface roughness is influenced by the feedstock powder, especially by particle size and particle morphology (Ref 12, 34). In addition to this, the surface roughness was reduced with higher temperature and gas pressure for both coating variants. The arithmetical mean heights (Sa) of the CGS coatings decreased from 19.1 (parameter set one) to 16.3 μm (parameter set four) for powder M3/2, while powder 316L displayed a reduction from 10.0 (parameter set one) to 9.7 μm (parameter set four). In this study, there was a linear relationship between particle velocity and the arithmetical mean height (Sa) for powder M3/2 with a coefficient of determination of $R^2_{\text{M3/2}} = 0.8478$. However, there was no linear relationship for powder 316L because the coefficient of determination was $R^2_{\text{316L}} = 0.1534$. For powder 316L, no influence of

Fig. 7 Arithmetical mean height (Sa) of the coating at different gas temperatures and gas pressures. Powder variants used: 316L and M3/2. Number of measurements = n . Error bars represent the standard deviation (1 sigma)

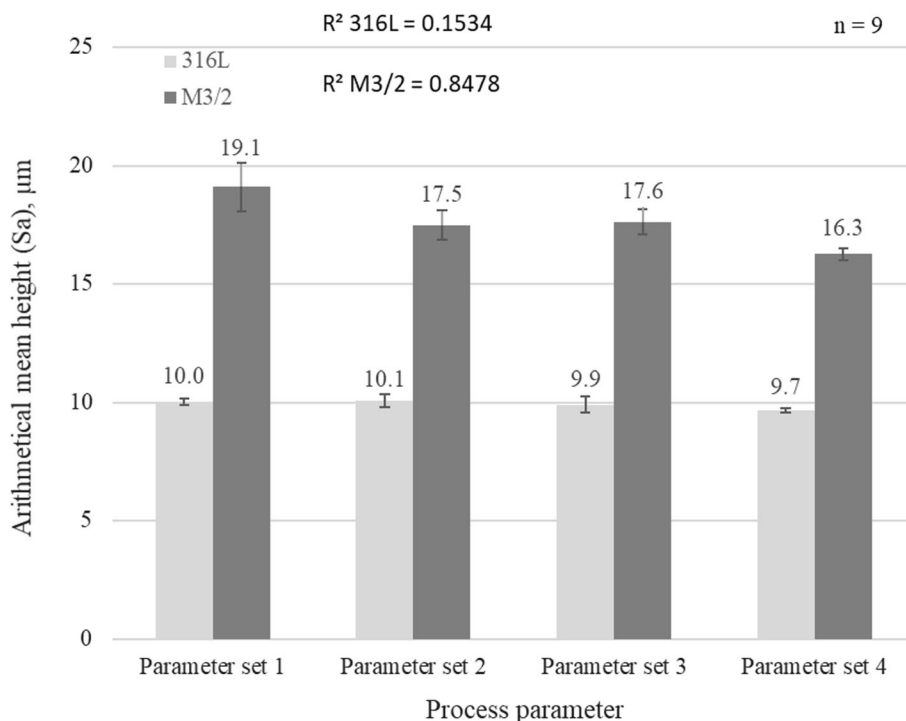
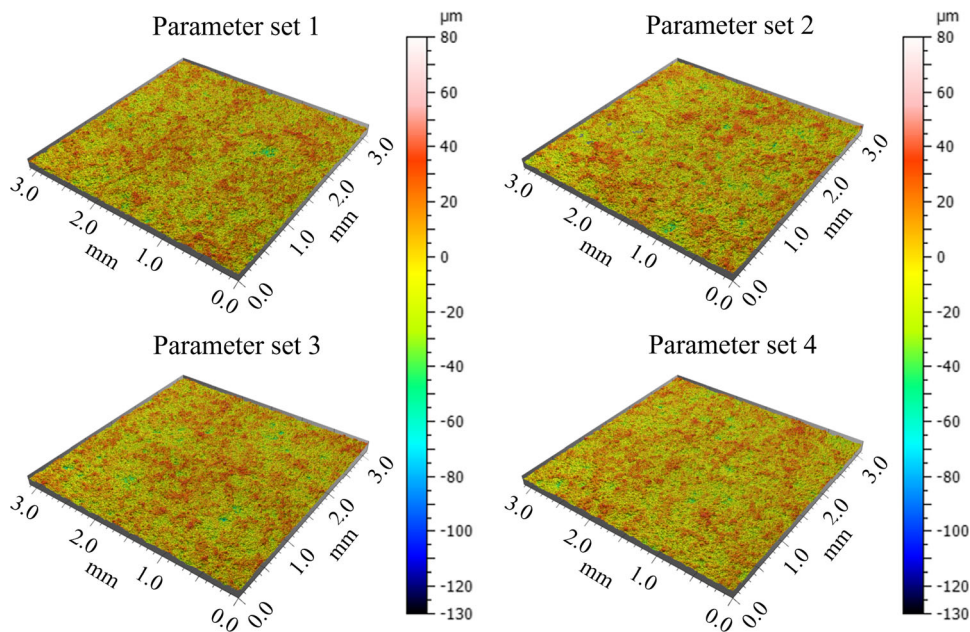


Fig. 8 3D representation of the CGS coating with powder 316L



different process parameters on the surface roughness was measurable. This could be due to the fact that coatings with small particle sizes already exhibit comparatively low surface roughness at low process parameters and the surface roughness hardly decreases with increasing process parameters (Ref 34).

In general, an increase in the utilized process parameters in CGS coatings increases the particle velocities.

Therefore, the plastic deformation of the particles on impact itself and the deformation process of the already underlying deposited particles also increase. Due to the high plastic deformation of the particles, the surface roughness of the CGS coating decreases, then (Ref 8, 34). This observation was also confirmed in the present investigation for CGS inner diameter coatings. With increasing process parameters, the surface roughness decreased for

Fig. 9 3D representation of the CGS coating with powder M3/2

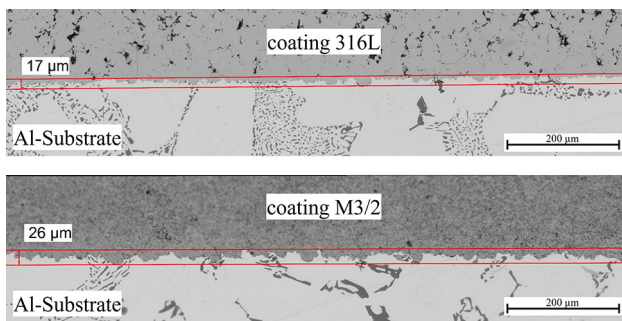
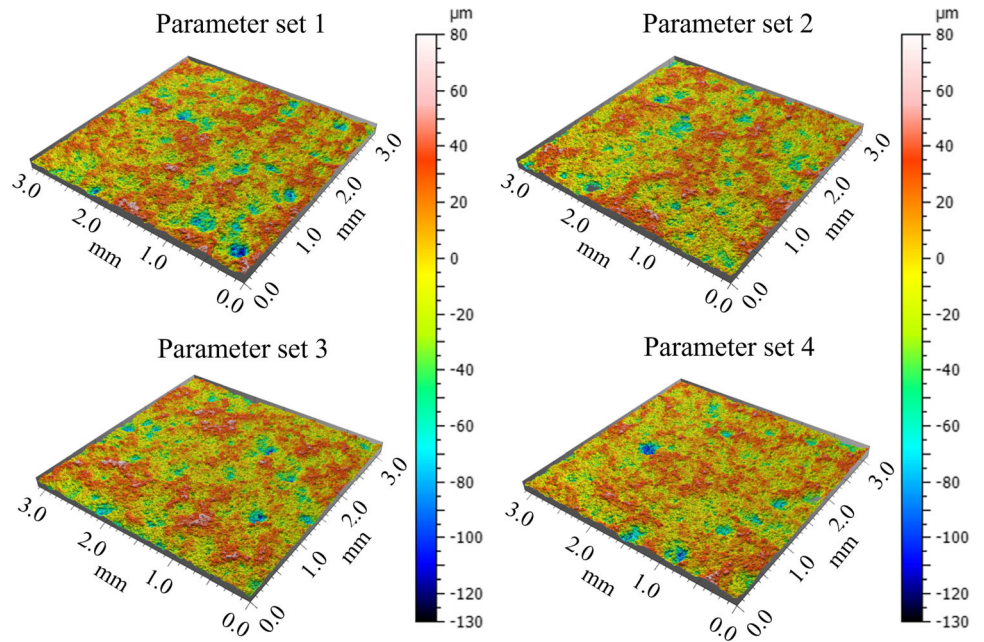


Fig. 10 Example of measuring the penetration depth of powder particles into the aluminum substrate using cross sections (parameter set one)

both powder variants. Coating M3/2 has a generally higher surface roughness compared to coating 316L due to the particle size.

Microstructure

Figure 10 shows the measurement of the penetration depth of the powder particles into the aluminum substrate using cross sections. Figure 11 highlights that the penetration depth of the powder particles was significantly higher for powder M3/2 than for powder 316L. No significant influence of different process parameters on the penetration depth of the powder particles into the substrate could be determined for both powder variants. The higher penetration depth of the M3/2 particles can be explained by the higher particle velocities in comparison with the velocities which can be attained with powder 316L (see Fig. 6). These results confirm previous investigations, which have

shown a strong relation between particle velocities and penetration depths of accelerated particles. The higher the particle velocity, the greater the plastic deformation on impact. As the velocities increase, the deformation of the particles and the substrate increases, too. Furthermore, a higher plastic deformation of the particles on impact leads to a higher penetration depth into the substrate (Ref 8, 23, 26, 34).

Figure 12 illustrates the correlation particle velocity and porosity. The measured porosity for coating 316L ranges from 5.6% (parameter 4) to 8.7% (parameter 1) and for coating M3/2 from 3.6% (parameter 4) to 4.8% (parameter 1). Furthermore, for both powder variants, the lowest porosity was measured for parameter 4 (highest particle velocity) and the highest for parameter 1 (lowest particle velocity). Porosity is influenced by powder size, powder morphology, process temperature and pressure and the resulting particle velocity. In general, the higher the process parameters, the higher the particle velocity and the lower the porosity (Ref 7, 38). This general statement also applies to the present results. No significant changes in porosity were measured over the height and circumference of the coated liner, indicating consistent coating quality. In addition, the coefficient of determination for the present results was determined. The coefficient of determination for powder 316L $R^2_{316L} = 0.8692$ is significantly higher than the coefficient of determination for powder M3/2 $R^2_{M3/2} = 0.6787$. The present results show a linear relationship between particle velocity and coating porosity for powder 316L. No linear relationship between velocity and porosity can be established for powder M3/2. Adhesion strength.

Fig. 11 Depth of penetration of the coating into the substrate at different gas temperatures and gas pressures. Powder variants used: 316L and M3/2. Number of measurements = n . Error bars represent the standard deviation (1 sigma)

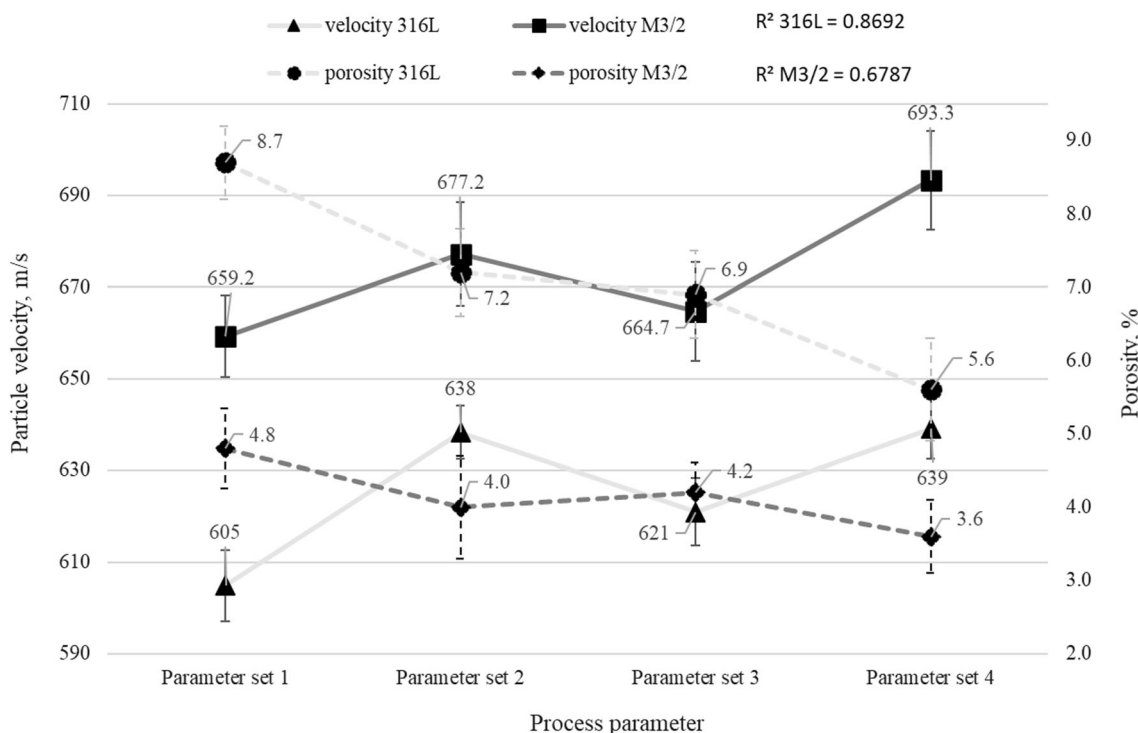
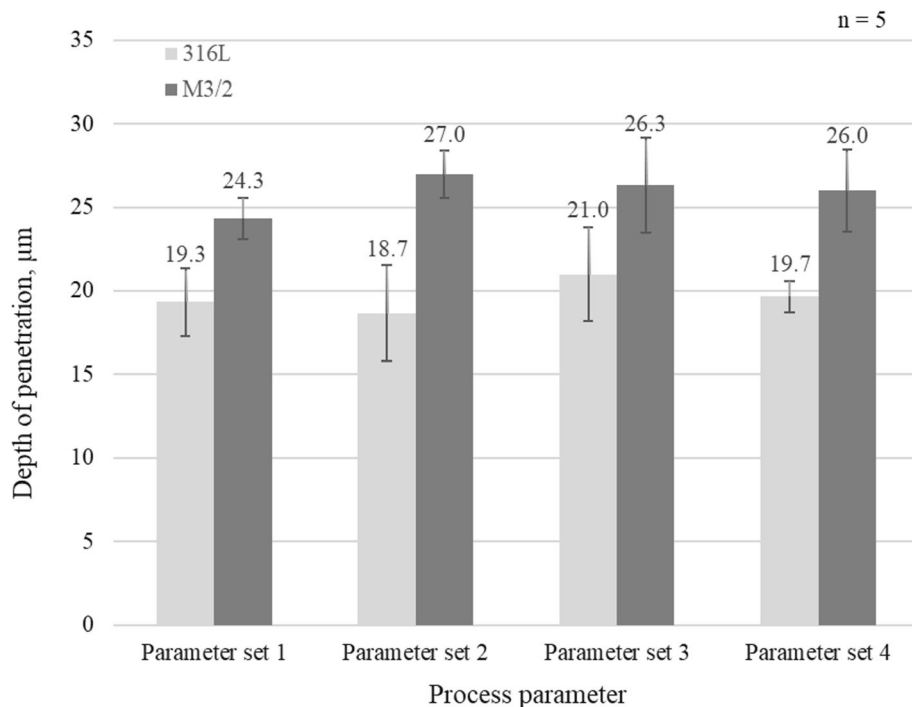


Fig. 12 Illustration of particle velocity and porosity at different process parameters (gas temperatures and gas pressures). Powder variants used: 316L and M3/2. Number velocity measurements

$n = 1000$. Number of porosity measurements $n = 12$. Error bars represent the standard deviation (1 sigma)

Figure 13 and 14 displays the results of the adhesion strength measurements. The coated liners were cut into small strips at 0°, 90°, 180° and 270° positions in order to measure the effects of the process parameters on the

circumference of the coated liners. Four dome-shaped stamps were glued onto each liner along the surface of the CGS coatings (see Fig. 2a). Two pull-off tests were performed for each powder variant and each parameter set.

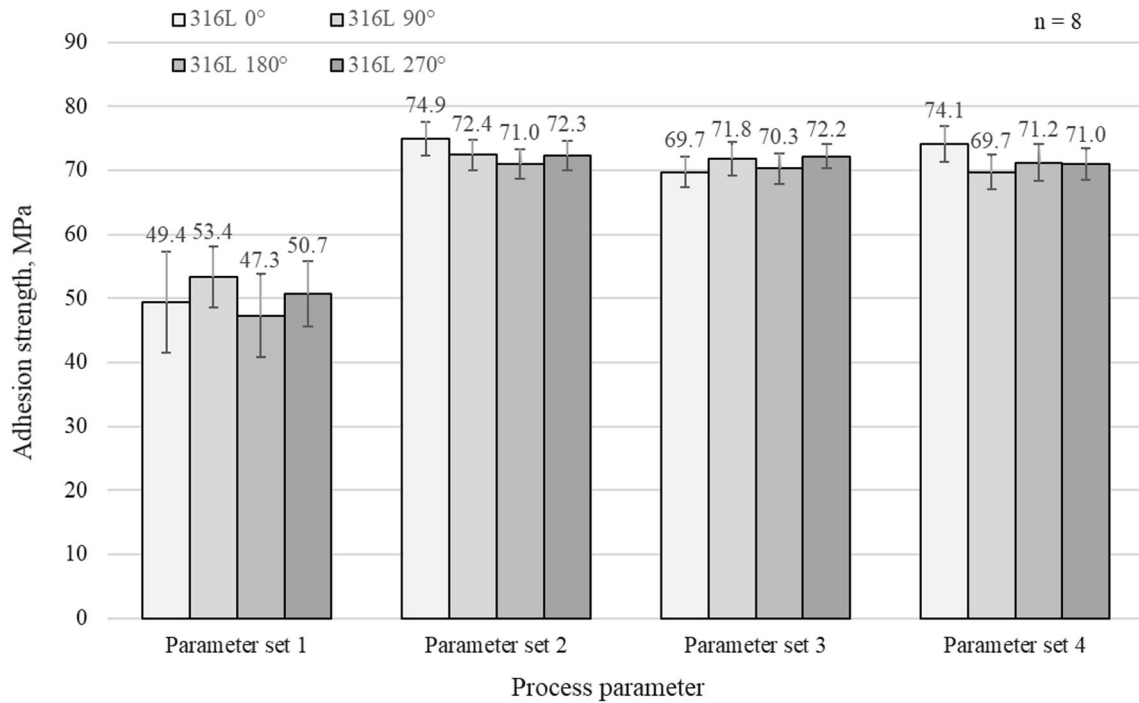


Fig. 13 Adhesion strength at different gas temperatures and gas pressures at different positions of the circumference (0°, 90°, 180° and 270°). Powder used: 316L. Number of measurements = *n*. Error bars represent the standard deviation (1 sigma)

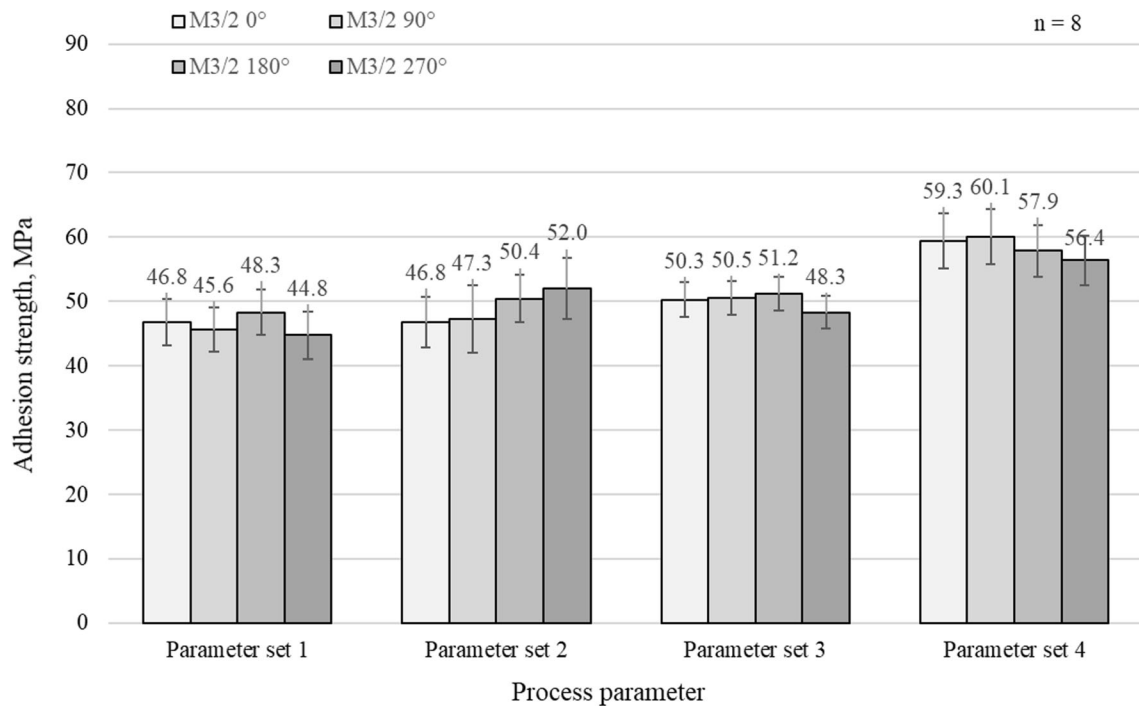


Fig. 14 Adhesion strength at different gas temperatures and gas pressures at different positions of the circumference (0°, 90°, 180° and 270°). Powder used: M3/2. Number of measurements = *n*. Error bars represent the standard deviation (1 sigma)

The positioning of the removal stamp had no influence on the adhesion strength.

The requirements of thermally coated cylinder bore surfaces in terms of adhesion strength is approximately 30 MPa in the automotive industry (Ref 39). This

minimum value for the adhesion strength was significantly exceeded for both powder variants in all applied process parameters. The measurements revealed that the adhesion strength of the CGS coating with powder 316L was higher than the coating with powder M3/2 in all parameters sets. Furthermore, removal experiments highlighted that the positioning of the removal stamp along the circumference (0° , 90° , 180° and 270°) had no significant influence on the quantified adhesion strengths. This indicates a consistent quality of the coating over the height and circumference of the liner. Therefore, only the adhesion strength values of the 0° position are examined in the following section.

The adhesion strength of the coating M3/2 was measured between 46.8 MPa (parameter set one and two) and 59.3 MPa (parameter set four). All measured values were below the maximum glue strength of approximately 70 MPa. Hence, cohesive failure of the coating M3/2 was observed in all tests. In contrast, the coatings of powder 316L displayed still adherent glue on the surfaces after removal with a maximum glue strength of 70 MPa in parameter set two to four. Thus, the bond in the glue failed awarding coatings with powder 316L an adhesion strength of approximately 70 MPa.

Figure 15 shows an exemplary test point of the adhesion strength measurements of three test liners as well as the dome-shaped stamps after an adhesion strength measurement: (a) coating 316L at parameter set one; (b) coating 316L at parameter set two; (c) coating M3/2 at parameter set one. Images (a) and (c) show cohesive failure of the CGS coatings since the coating still adheres to the liner and the dome-shaped stamp. Image (b) illustrates a failure of

the glue because a glue layer is still detectable on the stamp and the coated liner.

However, in parameter set one coating 316L showed a cohesive failure in the adhesion strength measurements which was similar to the M3/2 experiments. Due to that, a 14% increase in process pressure (parameter set one → parameter set two) or an 11% increase in process temperature (parameter set one → parameter set three) resulted in failure of the bonded glue when using 316L coatings.

The significant increase (up to 59.3 MPa) in the adhesion strength of coating M3/2 in parameter set four can be explained by the combined intensification of the process parameters (pressure: \uparrow 7 bar and temperature: \uparrow 100 °C). In addition, a significant increase of 52% in the adhesion strength of coating 316L (parameter set one → parameter set two) was also observed. The increase in adhesion strength is due to higher process parameters and thus ultimately to higher particle velocities (see Fig. 6). This study revealed that the generally valid statement—with increasing process parameters, the adhesion strength of the coating also increases—applies to internal coated CGS coatings, too. Furthermore, previous studies have shown that with increasing process temperature, the particle temperatures, and thus, the adhesion strength increases (Ref 5, 6, 23, 40, 41) This observation is also confirmed via the present investigation for CGS inner diameter coatings. The lower adhesive potential within the coatings of powder M3/2 is presumably due to the carbides in the powder and the hereby resulting lower plastic deformation of the particles. However, Fig. 11 shows that due to the high kinetic energy, the plastic deformation and therefore the

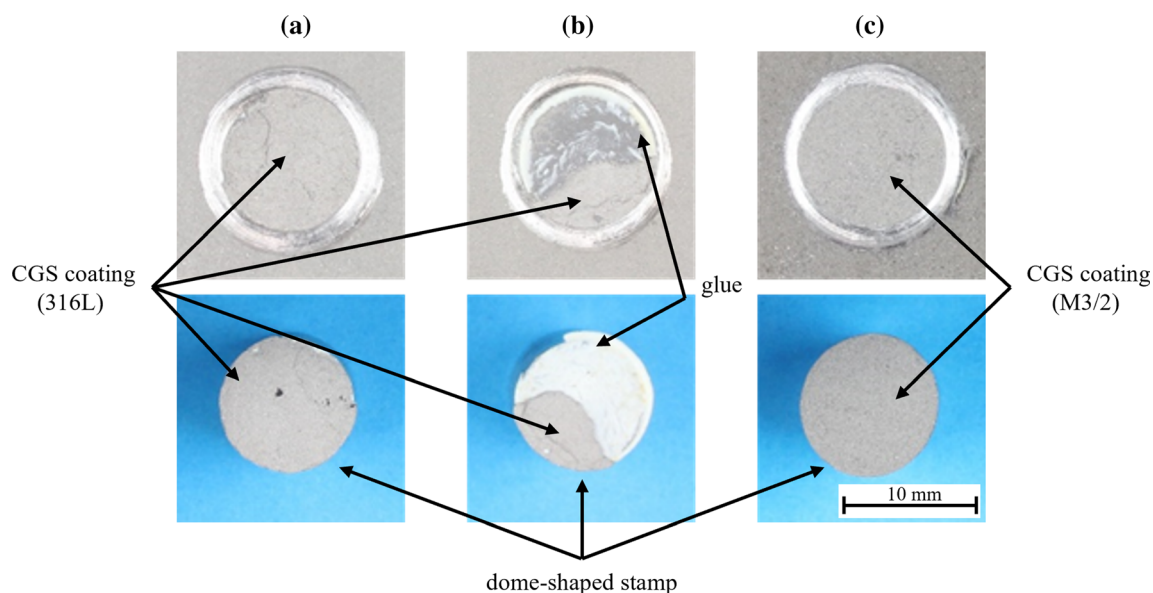


Fig. 15 Exemplary test point of the adhesion strength measurement of the liner as well as the dome-shaped stamp after the adhesion strength measurements: (a) coating 316L at parameter set one; (b) coating 316L at parameter set two; (c) coating M3/2 at parameter set one

penetration depth were higher for powder M3/2 than for powder 316L. In general, the amount of the particles' plastic deformation plays a critical role in regards to the penetration depth into the substrate and hereby ensures the coating's adherence to the substrate (Ref 42).

Conclusions

This study shows the influence of different process parameters on particle velocities, surface coating roughnesses, particle penetration depths into an aluminum substrate and adhesion strengths of CGS inner diameter coatings. Two different alloy steel powder variants (316L and M3/2) with different chemical compositions, particle sizes and morphologies were used. In summary, this research provides the following results:

- The larger the particle size of the feedstock powder, the greater the arithmetical mean height (S_a) of the manufactured CGS coating.
- When process parameters were increased (parameter set one to four), the surface roughness decreased by 15% for coatings with powder M3/2 and by 3% for coatings with powder 316L.
- Particles with higher particle velocities (M3/2 particles were 8% faster than 316L particles in parameter set four) penetrated 24% deeper into the substrate than particles with slower particle velocities.
- Powder 316L as well as powder M3/2 demonstrated sufficient adhesion strengths (> 30 MPa) for inner diameter coatings in the automotive industry when untreated cylindrical surfaces and process parameters with a minimum of 50 bar and 1000 °C are used.
- Increased process parameters led to higher particle velocities resulting in enhanced adhesion strengths of the fabricated CGS inner diameter coatings.
- The rotating CGS spray head was used to produce an inner diameter coating of consistent quality over the height and circumference of the liner. The position of the dome-shaped stamps along the circumference of the coated liner has no influence on the adhesion strength.

Acknowledgments The authors of this research would like to thank Reeti Singh and Jan Kondas from Impact Innovations GmbH for their support with the coating experiments.

Funding Open Access funding enabled and organized by Projekt DEAL.

Open Access This article is licensed under a Creative Commons Attribution 4.0 International License, which permits use, sharing, adaptation, distribution and reproduction in any medium or format, as long as you give appropriate credit to the original author(s) and the source, provide a link to the Creative Commons licence, and indicate

if changes were made. The images or other third party material in this article are included in the article's Creative Commons licence, unless indicated otherwise in a credit line to the material. If material is not included in the article's Creative Commons licence and your intended use is not permitted by statutory regulation or exceeds the permitted use, you will need to obtain permission directly from the copyright holder. To view a copy of this licence, visit <http://creativecommons.org/licenses/by/4.0/>.

References

1. A. Papyrin, V. Kosarev, S. Klinkov, A. Alkimov and V. Fomin, *Cold spray technology*, 1st ed. Elsevier, 2007.
2. T. Hussain, D.G. McCartney, P.H. Shipway and D. Zhang, Bonding Mechanisms in Cold Spraying: The Contributions of Metallurgical and Mechanical Components, *J. Therm. Spray Technol.*, 2009, **18**(3), p 364-379.
3. H. Assadi, F. Gärtner, T. Stoltenhoff and H. Kreye, Bonding mechanism in cold gas spraying, *Acta Mater.*, 2003, **51**(15), p 4379-4394.
4. W.-Y. Li, C.-J. Li and H. Liao, Effect of Annealing Treatment on the Microstructure and Properties of Cold-Sprayed Cu Coating, *J. Therm. Spray Technol.*, 2006, **15**(2), p 206-211.
5. D. Goldbaum, J.M. Shockley, R.R. Chromik, A. Rezaeian, S. Yue, J.-G. Legoux and E. Irissou, The Effect of Deposition Conditions on Adhesion Strength of Ti and Ti6Al4V Cold Spray Splats, *J. Therm. Spray Technol.*, 2012, **21**(2), p 288-303.
6. T. Schmidt, F. Gärtner, H. Assadi and H. Kreye, Development of a Generalized Parameter Window for Cold Spray Deposition, *Acta Mater.*, 2006, **54**(3), p 729-742.
7. S.H. Zahiri, W. Yang and M. Jahedi, Characterization of Cold Spray Titanium Supersonic Jet, *J. Therm. Spray Technol.*, 2009, **18**(1), p 110-117.
8. H. Assadi, H. Kreye, F. Gärtner and T. Klassen, Cold spraying – A materials perspective, *Acta Mater.*, 2016, **116**, p 382-407.
9. H. Assadi, T. Schmidt, H. Richter, J.-O. Kliemann, K. Binder, F. Gärtner, T. Klassen and H. Kreye, On Parameter Selection in Cold Spraying, *J. Therm. Spray Technol.*, 2011, **20**(6), p 1161-1176.
10. S. Dosta, G. Boilelli, A. Candeli, L. Lusvarghi, I.G. Cano and J.M. Guilemany, Plastic Deformation Phenomena During Cold Spray Impact of WC-Co Particles Onto Metal Substrates, *Acta Mater.*, 2017, **124**, p 173-181.
11. R. Maestracci, A. Sova, M. Jeandin, J.-M. Malhaire, I. Movchan, P. Bertrand and I. Smurov, Deposition of Composite Coatings by Cold Spray Using Stainless Steel 316L, Copper and Tribaloy T-700 Powder Mixtures, *Surf. Coat. Technol.*, 2016, **287**(4), p 1-8.
12. J. Meeß, M. Anasenzl, R. Ossenbrink, V. Michailov, R. Singh and J. Kondas, Cold Gas Spray Inner Diameter Coatings and Their Properties, *J. Therm. Spray Technol.*, 2022, **31**, p 1712-1724.
13. L. Aubanel, L. Lefeuvre, F. Delloro, M. Jeandin, and E. Sura, Cold spray coatings for automotive cylinder block application, in *ITSC 2019—Proceedings of the International Thermal Spray Conference*, (2019), pp. 433-440.
14. C.-J. Li, W.-Y. Li, Y.-Y. Wang, G.-J. Yang and H. Fukunuma, A Theoretical Model for Prediction of Deposition Efficiency in Cold Spraying, *Thin Solid Films*, 2005, **489**(1–2), p 79-85.
15. C.J. Li, G.J. Yang, C.X. Li, H. Bang, W.Y. Li, and others, Examination of the estimating approaches for the critical velocity in cold spraying, in *Thermal Spray 2007: Global Coating Solutions*, Eds. B. Marple, M. Hyland, Y.C. Lau, C.J. Li, R. Lima, and G. Montavon, May 14-16 (Beijing, China, 2007), ASM International, pp. 128-134

16. F. Gärtner, T. Stoltenhoff, T. Schmidt and H. Kreye, The Cold Spray Process and Its Potential for Industrial Applications, *J. Therm. Spray Technol.*, 2006, **15**(2), p 223-232.
17. A. Papyrin, S. Klinkov, and V. Kosarev, Modeling of particle-substrate adhesive interaction under the cold spray process, in *Thermal Spray 2003: Advancing the Science and Applying the Technology* Eds. B.R. Marple, C. Moreau, May 5-8 (Orlando, FL, 2003), ASM International, pp. 27-35
18. D. Zhang, P.H. Shipway and D.G. McCartney, Cold Gas Dynamic Spraying of Aluminum: The Role of Substrate Characteristics in Deposit Formation, *J. Therm. Spray Technol.*, 2005, **14**(1), p 109-116.
19. A.N. Papyrin, V. Kosarev, and S. Klinkov, Effect of the substrate surface activation on the process of cold spray coating formation, in *Thermal Spray 2005: Thermal Spray Connects: Explore Its Surfacing Potential!*, Ed. E. Lugscheider, May 24 (Basel, Switzerland, 2005), DVS-German Welding Society, pp. 145-150
20. C.-J. Li, W.-Y. Li and H. Liao, Examination of the Critical Velocity for Deposition of Particles in Cold Spraying, *J. Therm. Spray Technol.*, 2006, **15**(2), p 212-222.
21. F. Gartner, C. Borchers, T. Stoltenhoff, and H. Kreye, Numerical and microstructural investigations of the bonding mechanisms in cold spraying, in *Thermal Spray 2003: Advancing the Science and Applying the Technology*, Eds. B.R. Marple and C. Moreau, May 5-8 (Orlando, FL, 2003), ASM International, pp. 1-8
22. D.L. Gilmore, R.C. Dykhuizen, R.A. Neiser, T.J. Roemer and M.F. Smith, Particle Velocity and Deposition Efficiency in the Cold Spray Process, *J. Therm. Spray Technol.*, 1999, **8**(4), p 576-582.
23. R. Huang and H. Fukanuma, Study of the Influence of Particle Velocity on Adhesive Strength of Cold Spray Deposits, *J. Therm. Spray Technol.*, 2012, **21**(3-4), p 541-549.
24. M.F. Smith, J.E. Brockmann, R.C. Dykhuizen, D.L. Gilmore, R.A. Neiser and T.J. Roemer, Cold Spray Direct Fabrication - High Rate, Solid State, Material Consolidation, *MRS Online Proc. Libr.*, 1998, **542**, p 65-76.
25. J. Voyer, T. Stoltenhoff, and H. Kreye, Development of cold sprayed coatings, in *Thermal Spray 2003: Advancing the Science and Applying the Technology*, Eds. B.R. Marple and C. Moreau, May 5-8 (Orlando, FL, 2003), ASM International, pp. 71-78
26. S. Guetta, M.H. Berger, F. Borit, V. Guipont, M. Jeandin, M. Boustie, Y. Ichikawa, K. Sakaguchi and K. Ogawa, Influence of Particle Velocity on Adhesion of Cold-Sprayed Splats, *J. Therm. Spray Technol.*, 2009, **18**(3), p 331-342.
27. R. Fernández, D. MacDonald, A. Nastić, B. Jodoin, A. Tieu and M. Vijay, Enhancement and Prediction of Adhesion Strength of Copper Cold Spray Coatings on Steel Substrates for Nuclear Fuel Repository, *J. Therm. Spray Technol.*, 2016, **25**(8), p 1577-1587.
28. R.F. Vaz, A. Silvello, J. Sanchez, V. Albaladejo and I.G. Cano, The Influence of the Powder Characteristics on 316L Stainless Steel Coatings Sprayed by Cold Gas Spray, *Coatings*, 2021, **11**(2), p 168.
29. O.Ç. Özdemir, J.M. Conahan and S. Müftü, Particle Velocimetry, CFD, and the Role of Particle Sphericity in Cold Spray, *Coatings*, 2020, **10**(12), p 1254.
30. B. Jodoin, L. Ajdelsztajn, E. Sansoucy, A. Zúñiga, P. Richer and E.J. Lavernia, Effect of Particle Size, Morphology, and Hardness on Cold Gas Dynamic Sprayed Aluminum Alloy Coatings, *Surf. Coat. Technol.*, 2006, **201**(6), p 3422-3429.
31. J. Wu, H. Fang, S. Yoon, H. Kim and C. Lee, Measurement of Particle Velocity and Characterization of Deposition in Aluminum Alloy Kinetic Spraying Process, *Appl. Surf. Science*, 2005, **252**(5), p 1368-1377.
32. V.K. Champagne, D.J. Helfritch, S.P.G. Dinavahi and P.F. Leyman, Theoretical and Experimental Particle Velocity in Cold Spray, *J. Therm. Spray Technol.*, 2011, **20**(3), p 425-431.
33. S.P. Pardhasaradhi, V. Venkatachalapathy, S.V. Joshi and S. Govindan, Optical Diagnostics Study of Gas Particle Transport Phenomena in Cold Gas Dynamic Spraying and Comparison with Model Predictions, *J. Therm. Spray Technol.*, 2008, **17**(4), p 551-563.
34. V. Crespo, I.G. Cano, S. Dosta and J.M. Guilemany, The Influence of Feedstock Powders on the CGS Deposition Efficiency of Bond Coats for TBCs, *J. Alloys Compd.*, 2015, **622**, p 394-401.
35. M. Villa, S. Dosta and J.M. Guilemany, Optimization of 316L stainless steel coatings on light alloys using Cold Gas Spray, *Surf. Coat. Technol.*, 2013, **235**, p 220-225.
36. P. Richter, L. Holzgassner, J. Kondas and R. Singh, Advancements in Cold Spray-Equipment, Materials, and Selected Applications, in *11th Colloquium High Velocity Oxy-Fuel Flame Spraying*, Erding, Germany, 2018.
37. J. Pattison, S. Celotto, A. Khan and W. O'Neill, Standoff Distance and Bow Shock Phenomena in the Cold Spray Process, *Surf. Coat. Technol.*, 2008, **202**(8), p 1443-1454.
38. S.H. Zahiri, D. Fraser, S. Gulizia and M. Jahedi, Effect of Processing Conditions on Porosity Formation in Cold Gas Dynamic Spraying of Copper, *J. Therm. Spray Technol.*, 2006, **15**(3), p 422-430.
39. K. Bobzin, F. Ernst, K. Richardt, T. Schlaefler, C. Verpoort and G. Flores, Thermal spraying of cylinder bores With the Plasma Transferred Wire Arc process, *Surf. Coat. Technol.*, 2008, **202**(18), p 4438-4443.
40. T. Schmidt, F. Gaertner and H. Kreye, New Developments in Cold Spray Based on Higher Gas and Particle Temperatures, *J. Therm. Spray Technol.*, 2006, **15**(4), p 488-494.
41. Y. Watanabe, C. Yoshida, K. Atsumi, M. Yamada and M. Fukumoto, Influence of Substrate Temperature on Adhesion Strength of Cold-Sprayed Coatings, *J. Therm. Spray Technol.*, 2015, **24**(1-2), p 86-91.
42. T. Samson, D. MacDonald, R. Fernández and B. Jodoin, Effect of Pulsed Waterjet Surface Preparation on the Adhesion Strength of Cold Gas Dynamic Sprayed Aluminum Coatings, *J. Therm. Spray Technol.*, 2015, **24**(6), p 984-993.

Publisher's Note Springer Nature remains neutral with regard to jurisdictional claims in published maps and institutional affiliations.